Chinese Chemical Letters 35 (2024) 108434

Contents lists available at ScienceDirect

Chinese Chemical Letters

journal homepage: www.elsevier.com/locate/cclet

Restoring cellular calcium homeostasis to rescue ER stress by 1,2-bis(2-aminophenoxy)ethane-*N*,*N*,*N*′,*N*′-tetraacetic acid acetoxymethyl ester-loaded lipid-mPLGA hybrid-nanoparticles for acute kidney injury therapy

Jingwen Zhang[a,b,c,1], Jiahui Yan[a,b,1], Yanan Wang[a,b], Hong Liu[a,b], Xueping Sun[a,b], Yuchao Gu[c,*], Liangmin Yu[a,b,d], Changcheng Li[a,b,d], Jun Wu[e,f,*], Zhiyu He[a,b,d,*]

[a] *Frontiers Science Center for Deep Ocean Multispheres and Earth System, and Key Laboratory of Marine Chemistry Theory and Technology, Ministry of Education, Ocean University of China, Qingdao 266100, China*
[b] *College of Chemistry and Chemical Engineering, Ocean University of China, Qingdao 266100, China*
[c] *School of Medicine and Pharmacy, Ocean University of China, Qingdao 266003, China*
[d] *Sanya Oceanographic Institution, Ocean University of China, Qingdao 572024, China*
[e] *Bioscience and Biomedical Engineering Thrust, The Hong Kong University of Science and Technology (Guangzhou), Nansha, Guangzhou 511400, China*
[f] *Division of Life Science, The Hong Kong University of Science and Technology, Hong Kong 999077, China*

ARTICLE INFO

Article history:
Received 7 March 2023
Revised 1 April 2023
Accepted 4 April 2023
Available online 7 April 2023

Keywords:
BAPTA-AM
Calcium overload
Acid-responsive
AKI
ER stress

ABSTRACT

Early pathogenesis of ischemia-reperfusion (I/R)-induced acute kidney injury (AKI) is dominated by intracellular calcium overload, which induces oxidative stress, intracellular energy metabolism disorder, inflammatory activation, and a series of pathologic cascaded reactions that are closely intertwined with self-amplifying and interactive feedback loops, ultimately resulting in cell damage and kidney failure. Currently, most nanomedicines originate from the perspective of antioxidant stress, which can only quench existing reactive oxide species (ROS) but cannot prevent the continuous production of ROS, resulting in insufficient efficacy. As a safe and promising drug, BAPTA-AM is hydrolyzed into BAPTA by intracellular esterase upon entering cells, which can rapidly chelate with overloaded Ca^{2+}, restoring intracellular calcium homeostasis, thus inhibiting ROS regeneration at the source. Here, we designed a KTP-targeting peptide-modified yolk-shell structure of liposome–poly(ethylene glycol)methyl ether-*block*-poly (L-lactide-*co*-glycolic) (mPLGA) hybrid nanoparticles (<100 nm), with the characteristics of high encapsulation rate, high colloid stability, facile modification, and prolonged blood circulation time. Once the BA/mPLGA@Lipo-KTP was targeted to the site of kidney injury, the cholesteryl hemisuccinate (CHEMS) in the phospholipid bilayer, as an acidic cholesterol ester, was protonated in the simulated inflammatory slightly acidic environment (pH 6.5), causing the liposomes to rupture and release the BA/mPLGA nanoparticles, which were then depolymerized by intracellular esterase. The BAPTA-AM was diffused and hydrolyzed to produce BAPTA, which can rapidly cut off the malignant loop of calcium overload/ROS generation at its source, blocking the endoplasmic reticulum (ER) apoptosis pathway (ATF4–CHOP–Bax/Bcl-2, Casp-12–Casp-3) and the inflammatory pathway (TNF-α–NF-κB–IL-6 axes), thus alleviating pathological changes in kidney tissue, thereby inhibiting the expression of renal tubular marker kidney injury molecule 1 (Kim-1) (reduced by 82.9%) and also exhibiting prominent anti-apoptotic capability (TUNEL-positive ratio decreased from 40.2% to 8.3%), significantly restoring renal function. Overall, this research holds huge potential in the treatment of I/R injury-related diseases.

Acute kidney injury (AKI), a severe systemic syndrome, is characterized by a progressive decline in glomerular filtration rate (GFR) to less than 75%, abnormally elevated blood urea nitrogen (BUN) and creatinine (CRE), and a sharp decrease in urine output (less than 0.5 mL kg^{-1} h^{-1}) [1,2]. Without prompt management, the toxin continues to accumulate, resulting in dehydra-

* Corresponding authors.
E-mail addresses: guych@ouc.edu.cn (Y. Gu), junwuhkust@ust.hk (J. Wu), hezhiyu@ouc.edu.cn (Z. He).
[1] These authors contributed equally to this work.

https://doi.org/10.1016/j.cclet.2023.108434
1001-8417/

tion, electrolyte disturbances, and acid-base imbalance, which can eventually culminate in acute renal failure (ARF) with up to 50% in-hospital mortality [3,4]. However, no licensed pharmacological therapy offers a comprehensive, synergistic, and multifaceted improvement in the treatment of AKI. Clinically, renal replacement therapy (RRT), specifically hemodialysis and kidney transplantation, remain the only effective treatment choice for severe AKI. Moreover, RRT-related complications, such as infection induced by dialysis catheters, hemodynamic disorders, and immunological rejection following transplantation, are still unavoidable [5–7]. In the later stages of AKI, it is urgent to develop effective AKI drugs that may alleviate AKI in a short period (within a few hours) and promote the recovery of renal function, thus preventing the complications of AKI and the high mortality rate.

Renal ischemia-reperfusion (I/R)-induced AKI is prevalent in all types of cardiovascular disease (CVD), shock, acute renal artery occlusion, *etc.*, with an incidence of up to 60% in intensive care unit (ICU) patients [8,9]. The pathological mechanism of I/R-induced AKI is complex, involving intracellular calcium ion (Ca^{2+}) overload, oxidative stress, inflammatory activation, and cellular energy metabolism disorders, among which oxidative stress was once considered to be one of the most important contributors to the development of AKI [10]. Increasing evidence reveals that intracellular calcium overload is currently the dominant cause of oxidative stress. During I/R, the inflow of excessive extracellular Ca^{2+} and the efflux of endoplasmic reticulum (ER) Ca^{2+} will cause cytosolic Ca^{2+} overload [11,12]. Mitochondria, as the buffering center of intracellular Ca^{2+}, lead to mitochondrial dysfunction when continuously stimulated by a large amount of Ca^{2+} and then generate an abundance of reactive oxide species (ROS) [13]. The overproduction of ROS stimulates the ER membrane and the cell membrane, aggravating intracellular calcium overload and constituting a potent malignant feedback cycle [14]. Based on the aforementioned mechanisms, it is not difficult to conclude that an excess of Ca^{2+} seems to be the initial cause of cell death. Therefore, we anticipated that the rapid elimination of Ca^{2+} could restore mitochondrial function, alleviate oxidative stress, and inhibit inflammation, therefore efficiently curing AKI and restoring renal function. 1,2-Bis(2-aminophenoxy)ethane-*N*,*N*,*N*′,*N*′-tetraacetic acid acetoxymethyl ester (BAPTA-AM, BA-AM), a safe Ca^{2+}-selective chelator, does not chelate Ca^{2+} in the blood and can be hydrolyzed by esterases into the active Ca^{2+} chelator BA. Once BA enters cells, it will rapidly couple with Ca^{2+} to lower intracellular Ca^{2+} concentrations [15–18]. Currently, a number of studies have confirmed the therapeutic effect of metal ion chelation on diseases, indicating that this kind of therapy has the potential for clinical application [19,20]. We hypothesized that BA has great potential as an effective cell rescuer based on its excellent safety in blood circulation and efficient intracellular Ca^{2+} chelating ability. However, its clinical application is limited because BA-AM is a non-selective, extremely hydrophobic drug with low oral and intravenous bioavailability [15].

During renal ischemia, the intracellular oxygen content drops sharply, and the energy consumption of the cells becomes dependent on anaerobic respiration; consequently, a large amount of lactic acid accumulates in the AKI microenvironment [21–23]. Combined with the pathogenesis of AKI, it is possible to conclude that the disease microenvironment of AKI is characterized by slightly acid, high ROS, and overload with Ca^{2+}. In this study, the biodegradable polymer $mPEG_{2k}$-*b*-$PLGA_{75k}$ (mPLGA) was used to load BA-AM to obtain "yolk" BA-AM/mPLGA nanoparticles (BA-AM/mPLGA NPs), and then kidney targeting peptide (KTP) modified pH-responsive liposomes were used as "shells" to obtain BA-AM/mPLGA@Lipo-KTP hybrid NPs by a two-step nanocascade method (Scheme 1A). This design conferred on the hybrid drug delivery system the following characteristics (Scheme 1B): (i) High

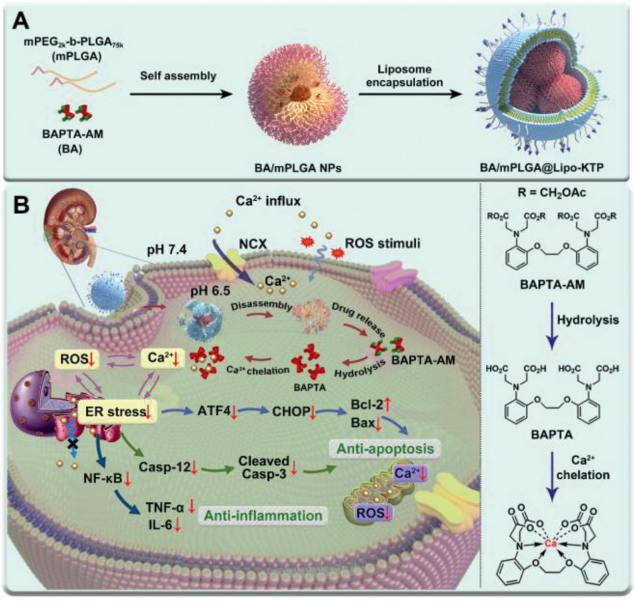

Scheme 1. The schematic illustration of the preparation route and the treatment mechanism of NPs. (A) Schematic diagram of the preparation of BA/mPLGA@Lipo-KTP. (B) The therapeutic mechanism of BA/mPLGA@Lipo-KTP in I/R-induced AKI rat model.

encapsulation efficiency (EE, up to 96.1%) and excellent physiological stability (~8 days): mPLGA polymer remedied the defects of low encapsulation efficiency and instability when liposomes encapsulate extremely hydrophobic drugs BA-AM [24–26]. (ii) Dual target characteristics: By adjusting the ratio of mPLGA to phospholipid, BA-AM/mPLGA@Lipo-KTP hybrid NPs were produced whose particle size could be controlled below 100 nm (~87.3 nm). This size had the characteristics of passively targeting the kidney, which can be filtered through the glomerular membrane, while few of them are captured by the liver and spleen [27]. In addition, the liposome "shell" modified with a KTP-targeting peptide (an elastin peptide with a unique CSAVPLC sequence) well compensates for the unmodifiable characteristics of mPLGA NPs, making it capable of actively targeting renal cells and promoting renal cell endocytosis [28,29]. (iii) pH-responsive drug release: The cholesteryl hemisuccinate (CHEMS) component in the phospholipid bilayer is an acidic cholesteryl ester, which changes its configuration in the simulated inflammatory slightly acidic environment (pH 6.5) to release the BA/mPLGA NPs, which further depolymerized to release BA-AM [30,31]. (iv) Source blocking therapy: BA-AM was decomposed by intracellular esterase to unleash BA, quickly removing intracellular excess Ca^{2+}, restoring calcium homeostasis, thus promoting the oxidative stress balance, playing anti-inflammatory and anti-apoptosis roles, finally promoting kidney function return. These as-prepared NPs have achieved remarkable results in the treatment of AKI, providing new opportunities for its future clinical application.

During the preparation of BA-loaded mPLGA NPs, we first adopted the flash nanocomplexation (FNC) micro-mixing method to turbulently mix the organic phase (DMSO) containing mPLGA and BA-AM with the aqueous phase (ddH_2O) (DMSO:ddH_2O:ddH_2O = 4:16:16) in a three-channel confined impinging jet (CIJ) microchamber in order to kinetically control the assembly process and form discrete BA/mPLGA NPs with high colloidal stability, uniform composition, and high drug loading efficiency. The BA/mPLGA NPs were subsequently coated with KTP-modified pH-responsive liposomes, yielding BA/mPLGA@Lipo-KTP NPs (Fig. 1A).

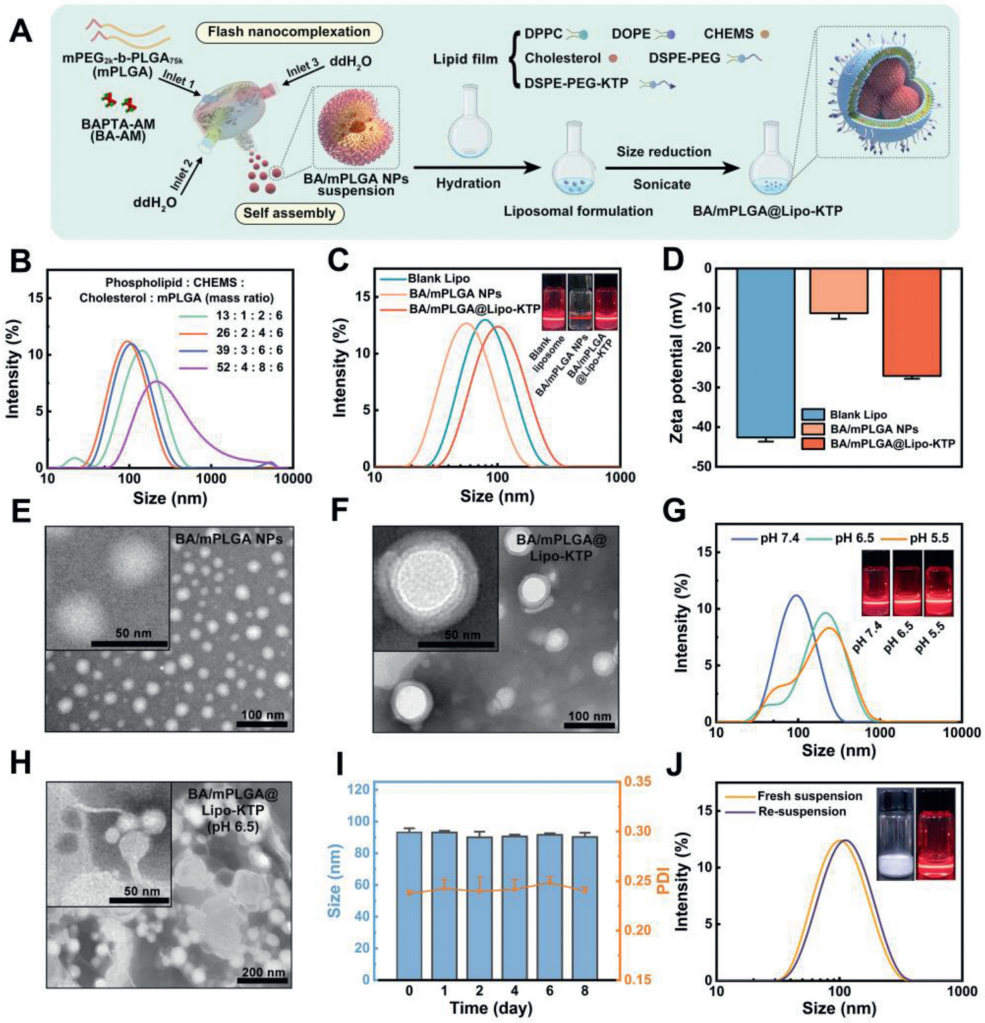

Fig. 1. Synthesis and characterization of BA/mPLGA@Lipo-KTP. (A) Schematic representation of the preparation of BA/mPLGA@Lipo-KTP. (B) Particle size distribution of BA/mPLGA@Lipo-KTP NPs prepared by different formulations. (C) Size distributions and photographs of the "Tyndall effect", and (D) ζ-potential of blank Lipo, BA/mPLGA NPs, and BA/mPLGA@Lipo-KTP. TEM images of (E) BA/mPLGA NPs and (F) BA/mPLGA@Lipo-KTP. (G) Size distributions and photographs of the "Tyndall effect" of BA/mPLGA@Lipo-KTP in simulated media [PBS with different pH (7.4, 6.5, or 5.5)] at 37 °C. (H) TEM image of BA/mPLGA@Lipo-KTP under simulated media (PBS: pH 6.5) incubated for 1 h. (I) Storage stability of BA/mPLGA@Lipo-KTP in PBS (pH 7.4, 10 mmol/L) for 8 days at 4 °C. (J) Size distributions of the BA/mPLGA@Lipo-KTP NPs before and after lyophilization, and photos of BA/mPLGA@Lipo-KTP lyophilized powder and "Tyndall effect" after re-suspended. Data are means ± standard deviation (SD), $n = 3$.

The synthesis of 1,2-distearyl-*sn*-glycerol-3-phosphoethanolamine-polyethylene glycol 2000-kidney target peptide (DSPE-PEG-KTP) (about 63.6 mg, yield rate: 83.3%, modification rate: 22.6%) was carried out by conjugating NH_2-KTP to 1,2-distearyl-*sn*-glycerol-3-phosphoglycolamine-polyethylene glycol 2000-*n*-hydroxysuccinimide (DSPE-PEG-NHS), as validated by proton nuclear magnetic resonance (^{1}H NMR). As depicted in Fig. S1 (Supporting information), the hydrogen spectra of DSPE-PEG-KTP exhibited the characteristic peaks of NH_2-KTP at 4.4 ppm and 0.9 ppm and DSPE-PEG-NHS at 1.23 ppm and 3.51 ppm, indicating that the peptide was successfully conjugated to DSPE-PEG-NHS. When the mass ratio of phospholipid/CHEMS/cholesterol/mPLGA was 13:1:2:6, the particle size distribution presented a multi-peak state, among which the small peak at 33.2 nm was distributed about 4.6%, which led to the hypothesis that insufficient phospholipid content leads to a small number of BA/mPLGA NPs not being encapsulated by liposomes (Fig. 1B). As liposome components (the proportion of CHEMS, cholesterol, and phospholipids remained unchanged) and content increased (the content of BA/mPLGA NPs remained unchanged), the particle size of the obtained BA/mPLGA@Lipo-KTP NPs gradually became larger, and the small peak of BA/mPLGA NPs disappeared. When the mass ratio of phospholipid/CHEMS/cholesterol/mPLGA was 26:2:4:6, the particle size of BA/mPLGA@Lipo-KTP was ~87.3 nm (<100 nm), which is favorable for passive targeting of the kidney, so we chose this mass ratio as the preparation parameter of subsequent NPs.

The dynamic light scattering (DLS) results (Fig. 1C) revealed that the hydrated radius of BA/mPLGA NPs was approximately 33.9 nm [polydispersity index (PDI): ~0.21], the hydrated radius of Blank Lipo was approximately 76.3 nm (PDI: ~0.17), and the hydrated radius of BA/mPLGA@Lipo-KTP was around 86.9 nm (PDI: ~0.21), indicating the successful encapsulation of BA/mPLGA by liposomes. Moreover, the "Tyndall effect" light path diagram revealed that these NPs in phosphate belanced solution (PBS) were dispersed uniformly (Fig. 1C), which facilitated their transport in the blood. The surface charges of Blank Lipo, BA/mPLGA NPs, and BA/mPLGA@Lipo-KTP were about −42.6, −11.3, and −27.1 mV, respectively, indicating that the liposome successfully packaged the surface of the BA/mPLGA (Fig. 1D). The negative surface charge of the NPs avoided their adsorption by proteins, hence contributing to the liposomes' excellent colloidal stability in blood circulation [32]. The transmission electron microscope (TEM) images

(Figs. 1E and F) revealed that BA/mPLGA NPs and BA/mPLGA@Lipo-KTP were spherical with good monodispersity and particle sizes of about 30 nm and 70 nm, respectively, which were slightly smaller than the hydration radius. In addition, the TEM image of BA/mPLGA@Lipo-KTP revealed the surface phospholipid bilayer structure, indicating that the liposomes were successfully packaged.

The EE of BA-AM in BA/mPLGA@Lipo-KTP was as high as 96.1%, demonstrating that the NPs could achieve high-efficiency loading of extremely hydrophobic drugs. When BA/mPLGA@Lipo-KTP was transferred from a simulated normal physiological environment (PBS, pH 7.4) to a simulated inflammatory, slightly acidic environment (PBS, pH 6.5 and 5.5), the particle size distribution changed from nanometers to microns (Fig. 1G). This was attributed to the disintegration of the liposome structure caused by the protonation of CHEMS, which induced fragments of BA/mPLGA@Lipo-KTP to aggregate. According to the "Tyndall effect" light path diagram, the BA/mPLGA@Lipo-KTP NPs' light path was disrupted under acidic conditions (pH 6.5 and 5.5), and visible solid particles were in motion. The TEM image of BA/mPLGA@Lipo-KTP after an acidic response (pH 6.5) further confirmed that the NPs' structure had been destroyed and aggregated (Fig. 1H). To further verify the protonation effect of CHEMS, we prepared liposomes by substituting an equal mass of cholesterol for CHEMS. By measuring the particle size in the normal physiological environment (pH 7.4) and slightly acidic environment (pH 6.5 and 5.5), as well as the photos and "Tyndall effect" light path diagram of NPs, we found that liposomes without CHEMS components were stable under acidic conditions, which indirectly verified that the original liposomes could be acid-responsive rupture due to the protonation of CHEMS (Fig. S2 in Supporting information).

Within 8 days, the particle size of the BA/mPLGA@Lipo-KTP remained ~90 nm and the PDI remained ~0.22 without drastic fluctuations, indicating that the NPs were stable at 4 °C for an extended period, which is favorable for future clinical use (Fig. 1I). We freeze-dried the BA/mPLGA@Lipo-KTP into powder and redissolved it in PBS, and the size distribution of the liposome was almost unchanged (from 89.7 nm to 92.3 nm), and its "Tyndall effect" light path was visible (Fig. 1J). According to the data presented above, NPs have long-term stability, and the preparation of the powder injection greatly reduces the difficulty of transportation, ensuring the feasibility of clinical treatment.

Next, at the cellular level, the biosafety of the BA/mPLGA@Lipo-KTP and its protective effect on injured cells were determined. As depicted in Figs. 2A and B, the cell viability of BA/mPLGA NPs and BA/mPLGA@Lipo-KTP was over 90% ($P > 0.5$) after co-incubation with HK-2 cells for 24 h over a BA-AM concentration range of 2.5 nmol/L to 400 nmol/L, indicating that neither BA/mPLGA NPs nor BA/mPLGA@Lipo-KTP exhibited cytotoxic effects on HK-2 cells. As shown in Fig. 2C, there was no visible hemolysis even when the concentration of BA-AM in the BA/mPLGA@Lipo-KTP reached 750 nmol/L, and the hemolysis rate was much lower than the threshold value (5%), confirming the safety of this nanoagent for blood transport [33,34].

As *in vitro* AKI cell models, HK-2 cells stimulated with hydrogen peroxide (H_2O_2) were used to explore the effects of NPs on intracellular Ca^{2+} levels, ROS levels, and cell necrosis levels. The intracellular Ca^{2+} level increased dramatically following H_2O_2 stimulation, almost 2 times that of normal cells, indicating a disruption of intracellular calcium homeostasis (Figs. 2D and E). There was no significant difference in intracellular Ca^{2+} levels between the empty liposome group and the model group, indicating that empty liposomes had no therapeutic effect. In comparison to the model group, the intracellular Ca^{2+} level in the free BA-AM (100 nmol/L) group decreased by 16.4%, whereas in the BA/mPLGA NPs (BA-AM concentration: 100 nmol/L) treatment group, the level of Ca^{2+} in the injured cells decreased by 41.1%. Since BA-AM is a hydrophobic drug, it is easy to aggregate and then precipitate in water-soluble media, thus hindering the uptake of drugs by cells. However, mPLGA NPs significantly improved the water solubility of BA-AM, promoting more drugs to enter the cell through endocytosis and finally playing the role of chelating intracellular Ca^{2+}. Furthermore, the Ca^{2+} chelation effect of BA/mPLGA@Lipo-KTP (BA-AM concentration: 100 nmol/L) was significantly superior to that of BA/mPLGA NPs (BA-AM concentration: 100 nmol/L), demonstrating that the encapsulation of a liposome can further promote cell internalization of BA-AM. When the BA-AM concentration in BA/mPLGA@Lipo-KTP was increased from 50 nmol/L to 100 nmol/L and then to 200 nmol/L, the Ca^{2+} level in the injured cells decreased continuously (from 37.3% to 28.1% and finally to 16.8%). When the concentration of BA-AM in BA/mPLGA@Lipo-KTP was 100 nmol/L, the Ca^{2+} level in the injured cells was not significantly different from that in the control group (26.7%). However, when the concentration of BA-AM was 200 nmol/L, the Ca^{2+} level in the injured cells was significantly lower than that in the control group.

Intracellular Ca^{2+} overload triggers the overproduction of ROS, which in turn stimulates the ER and cell membrane, leading to more Ca^{2+} flowing into the cytoplasm, thus aggravating the intracellular Ca^{2+} overload, forming a vicious cycle. After treatment with BA/mPLGA@Lipo-KTP at different concentrations (BA-AM concentration: 50, 100, and 200 nmol/L), the fluorescence intensity of ROS in damaged cells decreased by nearly 53.2%, 74.5%, and 63.8%, respectively, as compared to the model group, confirming that chelating overload Ca^{2+} could significantly reduce the intracellular ROS content. Moreover, when the Ca^{2+} concentration (BA/mPLGA@Lipo-KTP (BA-AM concentration: 200 nmol/L) group) was lower than the Ca^{2+} content of the control group, the ROS level rebounded further (from 11.3 to 18.9) (Figs. 2F and G), indicating that Ca^{2+} in the optimal concentration range can exert the most effective antioxidant effect.

The survival rates of cells treated with BA/mPLGA@Lipo-KTP (BA-AM concentration: 100 nmol/L) and BA/mPLGA@Lipo-KTP (BA-AM concentration: 200 nmol/L) were 93.4% and 82.1%, respectively, demonstrating that NPs could improve cell survival by chelating Ca^{2+} from the source (Fig. 2H), and further confirming that there was an optimal range of intracellular Ca^{2+} concentration mentioned above, which was consistent with the changing trend of ROS. To gain a more intuitive understanding of the effect of BA/mPLGA@Lipo-KTP on cell damage, live/dead cell labeling was used to evaluate cell viability (Figs. 2I and J). Compared to the model group, the live cell percentage of BA/mPLGA@Lipo-KTP (BA-AM concentration: 100 nmol/L) was up to 95%, which was consistent with the cell counting kit-8 (CCK-8) results. In conclusion, the appropriate concentration of BA/mPLGA@Lipo-KTP can rapidly chelate overloaded Ca^{2+}, thus precisely cutting off the source that promotes the continuous growth of ROS, which is conducive to restoring intracellular Ca^{2+} homeostasis, alleviating oxidative stress, in turn saving dying kidney cells.

To get closer to the clinical AKI process, we selected rats with bilateral renal artery clipping (40 min) as the AKI model to explore the therapeutic process of the NPs *in vivo*. The animal experiment was approved by the Institutional Animal Care and Use Committee of the Ocean University of China. As depicted in Fig. S3 (Supporting information), after the renal artery was clamped, the kidney's color changed to gray, indicating that renal blood flow occlusion was successful. After 40 min of ischemia, the renal artery clamp was removed, and the kidney quickly returned to its normal light reddish-brown color within 5 min, suggesting successful reperfusion. Rats with AKI were treated according to the timeline shown in Fig. 3A.

The accumulation of NPs in the kidney is a prerequisite for AKI treatment. Therefore, DiR/BA/mPLGA@Lipo and

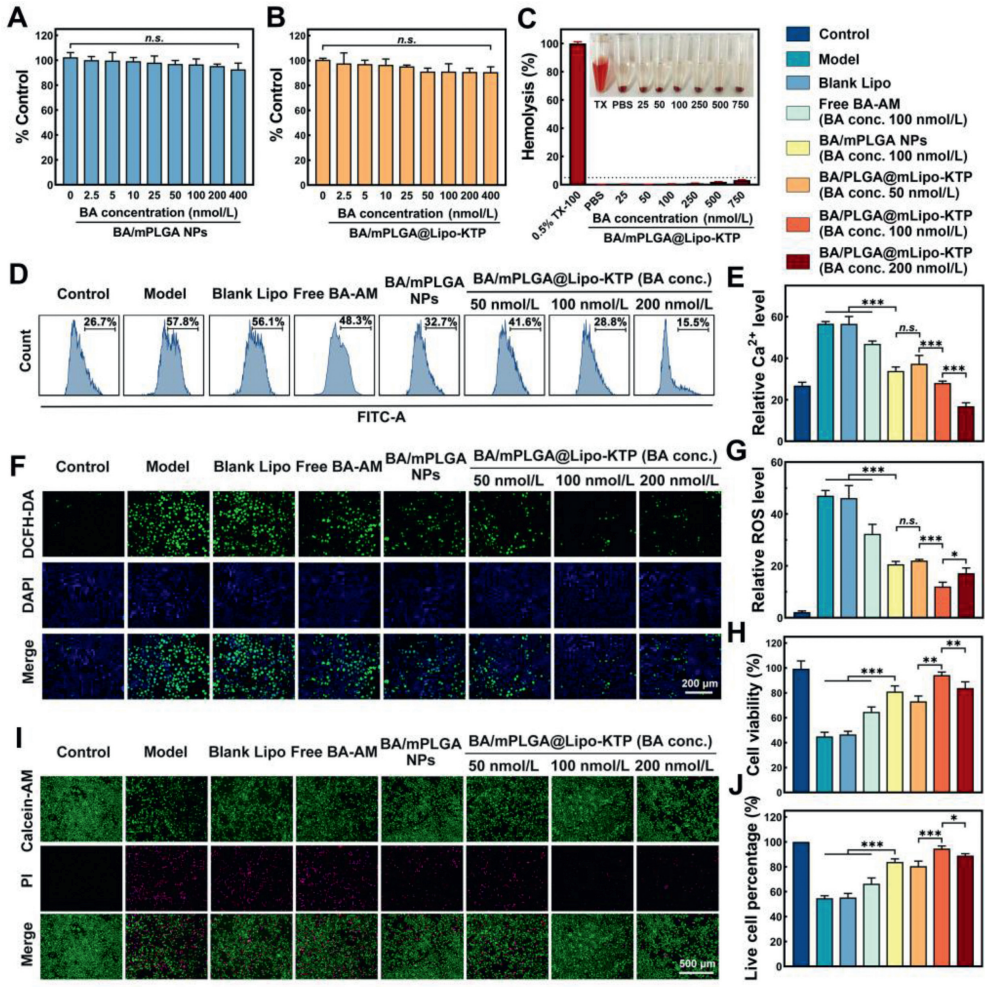

Fig. 2. Cellular protective effect of BA/mPLGA@Lipo-KTP. The cell viability (CCK-8) of HK-2 cells was incubated with different doses of (A) BA/mPLGA NPs and (B) BA/mPLGA@Lipo-KTP for 24 h. (C) Relative hemolysis ratio of various concentrations of BA/mPLGA@Lipo-KTP. The pretreatment process of the following experiments is consistent, and the specific operation is as follows: H_2O_2-stimulated HK-2 cells were incubated with PBS, blank Lipo, free BA-AM (100 nmol/L), BA/mPLGA NPs (BA-AM: 100 nmol/L), BA/mPLGA@Lipo-KTP (BA-AM: 50, 100, and 200 nmol/L) for 12 h, respectively. (D) Flow cytometry results and (E) semi-quantitative flow cytometry results of Ca^{2+} level in H_2O_2-stimulated HK-2 cells with different treatments. (F) Fluorescence images and (G) semi-quantitative results of intracellular ROS. (H) The cell viability (CCK-8) of H_2O_2-induced HK-2 cells after various NPs treatments. (I) Fluorescence images and (J) semi-quantitative results of AM/PI-stained injured HK-2 cells after 12 h of treatment. Data are mean ± SD, $n = 6$. $^{*}P < 0.05$, $^{**}P < 0.01$, $^{***}P < 0.001$. *n.s.*, no significance.

DiR/BA/mPLGA@Lipo-KTP were administered intravenously into AKI rats to visualize the distribution of NPs *in vivo*. As shown in Fig. 3B and Fig. S4 (Supporting information), the fluorescence intensity of DiR/BA/mPLGA@Lipo-KTP (BA-AM concentration: 200 μg/kg *bw*) in the kidney at 1, 3, and 6 h was 1.4, 1.3, and 1.2 times that of DiR/BA/mPLGA@Lipo, respectively, indicating that KTP can assist NPs in preferentially recognizing kidney cells and thus provide support for the effective accumulation of NPs in the kidney site. Besides, the partial accumulation of NPs in the liver and spleen was due to the fact that these organs are part of the mononuclear phagocyte system and capture some NPs during toxin filtration.

As shown in Fig. S5 (Supporting information), the renal coefficient of the model group was significantly higher than that of the normal group, indicating that severe congestion and edema occurred in the renal tissue. After treatment with BA/mPLGA@Lipo-KTP (200 μg/kg *bw*) for 24 h, the renal coefficient was lower than that in the model group ($P < 0.05$), showing that the nanodrug could protect kidney cells from damage and reduce renal edema. Compared to the model group, the level of Ca^{2+} in the kidney tissue of AKI rats treated with BA/mPLGA NPs decreased by ~21.3%, indicating that BA-AM chelated the excess of Ca^{2+} in the injured kidney cells, thus inhibiting the development of AKI at its source (Fig. 3C). After BA/mPLGA@Lipo-KTP treatment, the Ca^{2+} content decreased by up to ~40.3%, which was not significantly different from the control group, indicating that the liposome shell modified with the targeted peptide KTP increased the blood circulation time of drugs and improved the efficiency of targeted drug delivery.

CRE and BUN are two key indicators for evaluating renal excretory function clinically [35]. As shown in Figs. 3D and E, 12 h after reperfusion, the CRE and BUN levels of rats in the model group were 5 and 9 times those of the control group, respectively, suggesting the destruction of kidney function. After 12 h of treatment with BA/mPLGA (BA-AM concentration: 200 μg/kg *bw*), CRE and BUN levels decreased by 40.1% and 36.5%, respectively, compared to the model group, and in the BA/mPLGA@Lipo-KTP (BA-AM concentration: 200 μg/kg *bw*) treatment group, CRE and BUN levels decreased by 68.3% and 75.5%, respectively. Moreover, following 24 h of treatment with BA/mPLGA@Lipo-KTP, CRE and BUN levels were lowered by 83.8% and 91.3%, respectively, and almost restored to normal levels, suggesting that NPs themselves had a beneficial effect on alleviating kidney injury. We believe that the main reason for the restoration of renal function by BA/mPLGA@Lipo-KTP

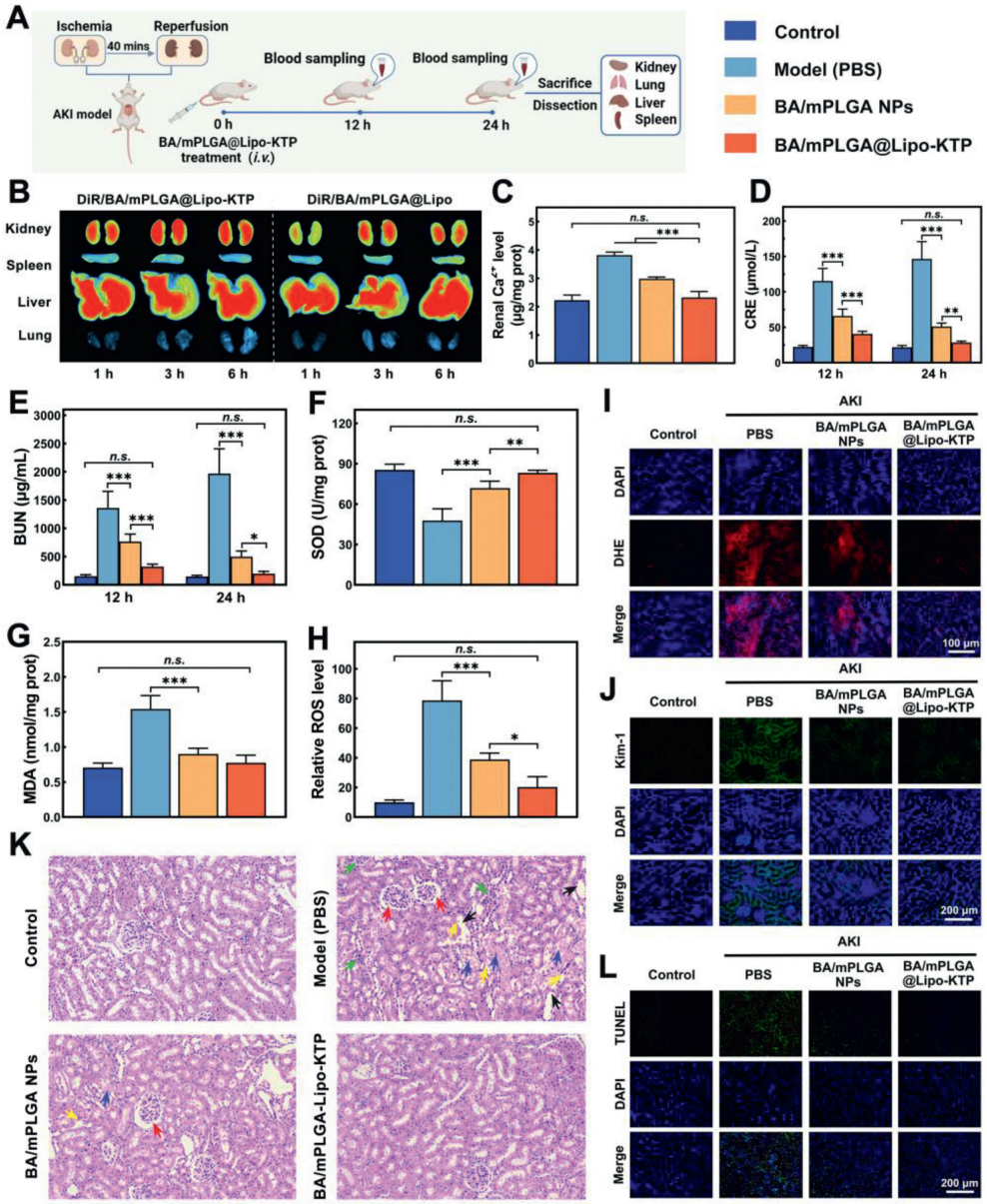

Fig. 3. *In vivo* therapeutic effect in I/R-induced AKI rat model. (A) Experimental flowchart of the AKI rat model treatment process. (B) The *ex vivo* near-infrared (NIR) imaging of major organs (liver, spleen, lungs, and kidneys) in AKI rats. Data are mean ± SD, $n = 3$. (C) Renal Ca^{2+} level, blood serum (D) CRE, (E) BUN, (F) SOD, and (G) MDA levels from each group. (H) DHE fluorescence semi-quantitative and (I) staining results of kidney tissues in different groups. (J) Immunostaining of Kim-1. (K) H&E staining of kidney tissues in different groups. Green arrows indicate inflammatory cell infiltration, black arrows indicate renal tubular dilatation; yellow arrows indicate renal tubular epithelial cell exfoliation site; blue arrows indicate necrotic shedding of renal tubular epithelial cells to form casts; and red arrows indicate glomerulus pyknosis. (L) Terminal deoxynucleotidyl transferase dUTP nick end labeling (TUNEL) staining of kidney tissues in different groups. Data are mean ± SD, $n = 6$. $^{*}P < 0.05$, $^{**}P < 0.01$, $^{***}P < 0.001$.

was that BA effectively chelated the overloaded Ca^{2+} in the cytoplasm, thereby restoring calcium homeostasis and cutting off the ROS production pathway.

The superoxide dismutase (SOD) is a natural superoxide-free radical scavenging agent in the body that can decompose harmful superoxide free radicals and preserve the redox balance of the body [36]. The SOD level in the model group was nearly reduced in half (48.9%) compared to the normal group, indicating that the ability of damaged kidneys to remove free radicals was severely diminished (Fig. 3F). The antioxidant capacity of damaged kidneys treated with BA/mPLGA NPs was 1.5 times that of the model group, indicating that BA-AM could inhibit ROS production by chelating Ca^{2+} and restore the kidney's antioxidant capacity. In addition, there was no significant difference in SOD level between the AKI models treated with BA/mPLGA@Lipo-KTP and the normal group. This may be due to the fact that the liposome shell not only prolongs the circulation time of circulating blood but also has the ability of active targeting, thereby delivering more BA-AM to the injured kidney site, blocking the generation of ROS, and promoting the kidney antioxidant system to return to normal. MDA is the ultimate product of lipid oxidation, which can aggravate membrane damage, therefore, determining its level can more accurately indicate the degree of lipid peroxidation and indirectly reflect the degree of cell damage [37]. The level of malondialdehyde (MDA) in the model group was significantly elevated (more than twice that of the normal group), whereas the level of MDA in the kidneys of AKI rats treated with BA/mPLGA@Lipo-KTP was decreased by 53.1%, showing no significant difference from that in the normal group, indicating that the peroxidation of the damaged kidney tissue was inhibited (Fig. 3G).

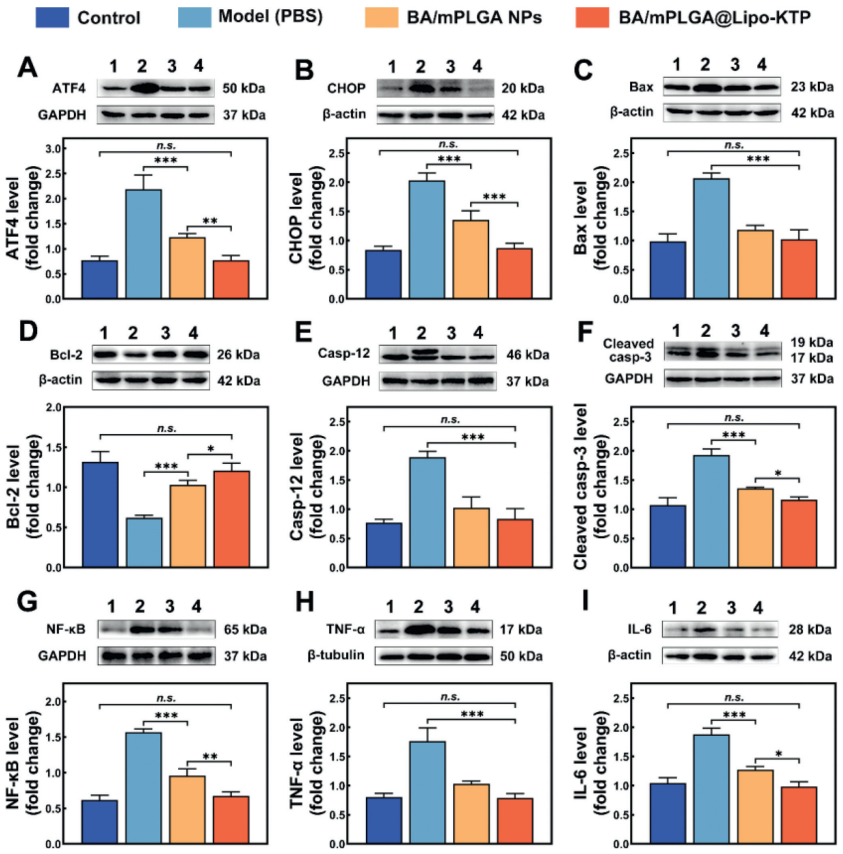

Fig. 4. *In vivo* therapeutic mechanisms. Western blot (WB) analysis of (A) ATF4, (B) CHOP, (C) Bax, (D) Bcl-2, (E) Casp-12, (F) cleaved Casp-3, (G) NF-κB, (H) TNF-α, and (I) IL-6 expression and the semi-quantitative results. 1–5 represents the control group, AKI (PBS) group, blank Lipo group, BA/mPLGA NPs group, and BA/mPLGA@Lipo-KTP group, respectively. GAPDH, glyceraldehyde-3-phosphate dehydrogenase. Data are mean ± SD, $n = 3$. $^{*}P < 0.05$, $^{**}P < 0.01$, $^{***}P < 0.001$.

To further explore the antioxidant effect of the NPs at the tissue level, we evaluated the overall oxidation of the kidney using dihydroethidium (DHE) staining (Figs. 3H and I). The fluorescence intensity (red fluorescence) of DHE in the kidney of AKI rats treated with BA/mPLGA@Lipo-KTP was reduced by 70.6% compared to the model group (the tissue oxidation level was 8.5 times higher than that in the normal group), which was consistent with the experimental results of ROS at the cellular level. After treatment with BA/mPLGA@Lipo-KTP, the kidney oxidation level of rats with AKI returned to normal, which was primarily due to the chelation of Ca^{2+}, which inhibited the mass production of ROS and restored the kidney's antioxidant properties.

Kidney injury molecule 1 (Kim-1) is a new type I transmembrane glycoprotein that is almost not expressed in the kidney under normal conditions. However, Kim-1 expression increased significantly within hours after kidney injury [38,39]. As shown in Fig. 3J and Fig. S6 (Supporting information), the expression level of Kim-1 in the AKI model group was over 70 times that of the normal group, and it was mostly concentrated in the renal tubules, indicating that ischemia and reperfusion caused serious damage to renal tubule cells. Furthermore, after treatment with BA/mPLGA@Lipo-KTP, Kim-1 expression decreased by 82.9%, demonstrating that BA can rapidly chelate overloaded Ca^{2+}, thus reducing renal tubule cell damage.

To further explore the improvement of BA/mPLGA@Lipo-KTP on injured nephrons, hematoxylin-eosin (H&E) staining was performed on the kidneys of different treatment groups to observe the pathological changes (Fig. 4K). The model group exhibited typical AKI histological features, such as renal tubule dilatation (black arrow), glomerulus pyknosis (red arrow), necrotic shedding of renal tubular epithelial cells to form casts (blue arrow), renal tubular epithelial cell exfoliation (yellow arrow), and increased inflammatory cell infiltration (green arrow). In contrast, treatment with BA/mPLGA NPs resulted in only minor tubular cell damage and renal tubule dilatation, and the nephron damage was reversed dramatically. Surprisingly, after treatment with BA/mPLGA@Lipo-KTP, no evident histopathological features of AKI were observed in the kidney tissue, providing sufficient support for the restoration of kidney structure and function with BA/mPLGA@Lipo-KTP.

In the final stage of AKI, a large number of proximal tubule apoptosis events occur, promoting nephron loss and ultimately accelerating the occurrence and progression of renal failure. As shown in Fig. 3L and Fig. S7 (Supporting information), compared with the model group (the positive rate of apoptosis reached 42.3%), the apoptosis rate of BA/mPLGA NPs treatment decreased to 17.3%, and that of BA/mPLGA@Lipo-KTP treatment decreased more significantly (~8.2%), which was close to the normal level. These results indicated that the preparation can effectively prevent the massive apoptosis of renal cells, thereby reducing the risk of renal failure.

Intracellular Ca^{2+} overload and ROS overproduction are two key factors in AKI, and their subsequent activation of ER stress (ERS) is the decisive factor that ultimately leads to renal cell death. Moreover, the production of inflammatory factors during AKI can also accelerate the apoptosis of renal cells. As a result, we explored its anti-apoptotic and anti-inflammatory mechanisms from the following two aspects.

As the largest intracellular Ca^{2+} store, ER is essential for maintaining the balance of cellular calcium concentration by integrating and regulating Ca^{2+} uptake, release, and binding processes. In AKI,

disruption of ER calcium homeostasis causes the accumulation and aggregation of unfolded proteins, resulting in severe ERS [40,41]. On the one hand, ERS increases protein kinase R-like ER kinase (PERK) activity; PERK phosphorylates eukaryotic translation initiation factor 2α (eIF2α), inhibits protein translation and synthesis, and relieves ER pressure [42]. At the same time, phosphorylation of eIF2α can selectively initiate recombinant activating transcription factor 4 (ATF4) translation, increase the synthesis of its binding ligand, affect amino acid metabolism, and inhibit protein translation and synthesis [43]. ATF4 also promoted the expression of the transcription factor C/EBP-homologous protein antibody (CHOP), which inhibited the expression of the anti-apoptotic protein Bcl-2, activated the expression of the pro-apoptotic protein Bax, and finally induced endogenous apoptosis [44,45]. On the other hand, ERS activates Casp-12, which further triggers cytoplasmic Casp-3 activation *via* cleavage and activation of Casp-9, ultimately leading to apoptosis [46].

As shown in Fig. 4A, the expression level of ATF4 in the model group was 3.2 times that of the normal group, confirming the activation of the PERK pathway in the injured kidney. After treatment with BA/mPLGA NPs, the expression of ATF4 decreased by approximately 47.9%, indicating that calcium chelation by BA inhibited the activation of the PERK pathway. In addition, the expression of ATF4 decreased by 68.9% after treatment with BA/mPLGA@Lipo-KTP, which is close to the normal level, indicating that BA/mPLGA NPs coated with liposomes modified with kidney-targeting peptides can prolong the drug cycle, resulting in more NPs targeting to the lesion site, thus inhibiting ERS signal transduction thoroughly. As can be seen from Fig. 4B, compared with the model group, after BA/mPLGA@Lipo-KTP treatment, the expression of CHOP, the apoptotic initiation signal regulated by the upstream signal ATF4, decreased by about 54.5%, indicating that our NPs were able to block the upstream signal at its source, thus reducing the possibility of downstream apoptotic protein upregulation. As shown in Figs. 4C and D, the expression level of Bax (a pro-apoptotic protein) in the model group was about twice that of the normal group, whereas the expression level of Bcl-2 (an anti-apoptotic protein) was decreased by 53.6%. The expression of Bax was significantly lowered by 47.6% and the expression of Bcl-2 was significantly increased by 2.1 times following treatment with BA/mPLGA@Lipo-KTP. In addition, we compared the ratio of Bcl-2 to Bax. The higher the ratio, the stronger the ability of cells to anti-apoptosis. As shown in Fig. S8 (Supporting information), the BA/mPLGA@Lipo-KTP treatment greatly strengthened the anti-apoptotic capability of cells in AKI rats, with the Bcl-2/Bax ratio increasing to around 5.4 times that of the model group, recovering to a level comparable to that in the normal group.

Moreover, as shown in Fig. 4E, the expression level of the ERS-activated apoptotic factor Casp-12 in the AKI rat model group was about 2.8 times that of the control group, and after treatment with BA/mPLGA@Lipo-KTP, Casp-12 expression was significantly inhibited, decreasing by about 60.9%. Cleaved Casp-3 expression was further suppressed by the down-regulation of Casp-12. As shown in Fig. 4F, the BA/mPLGA@Lipo-KTP treatment decreased the expression of cleaved Casp-3 by 42.5% compared to the model group, showing no significant difference from that in the normal group.

In brief, BA/mPLGA@Lipo-KTP chelate overloaded Ca^{2+} from the source, which can significantly inhibit the expression of the key proteins of ERS–PERK signal axis (ATF-4-CHOP), further inhibit the expression of pro-apoptotic protein Bax, and restore the expression of anti-apoptotic protein Bcl-2. In addition, BA/mPLGA@Lipo-KTP also inhibited the expression of Casp-12 induced by ERS and blocked the up-regulation of Casp-3, protecting the kidney and promoting the normalization of kidney function.

In additional, during AKI, intracellular calcium overload, and ROS overproduction activate the nuclear factor-k-gene binding (NF-κB) pathway and stimulate the release of a large number of inflammatory factors [tumor necrosis factor-α (TNF-α), NF-κB, interleukin 6 (IL-6), IL-1β, *etc.*] [47]. As shown in Fig. 4G, the expression of NF-κB was 2.6 times higher in the model group than that in the normal group but decreased by 31.3% in the BA/mPLGA NPs treatment group. There was no significant difference in the expression of NF-κB between the BA/mPLGA@Lipo-KTP treatment group and the normal group. As shown in Figs. 4H and I, the expressions of TNF-α and IL-6 in the model group were 2.5 times and 1.8 times of those in the control group, respectively, whereas, after treatment with BA/mPLGA NPs, the expressions of TNF-α and IL-6 decreased by 50.3% and 37.5%, respectively. Besides, there was no significant difference between the expression levels of TNF-α and IL-6 in the group treated with liposome-coated BA/mPLGA NPs and the normal group, further indicating that the drug with targeted liposome encapsulation could reach more lesion sites and thus play anti-inflammatory effects. The reduced levels of NF-κB, TNF-α, and IL-6 demonstrated that the nanoagent further inhibited the inflammatory response, consequently inhibiting the expression of the apoptotic executive Casp-3 and rescuing the endangered kidney cells.

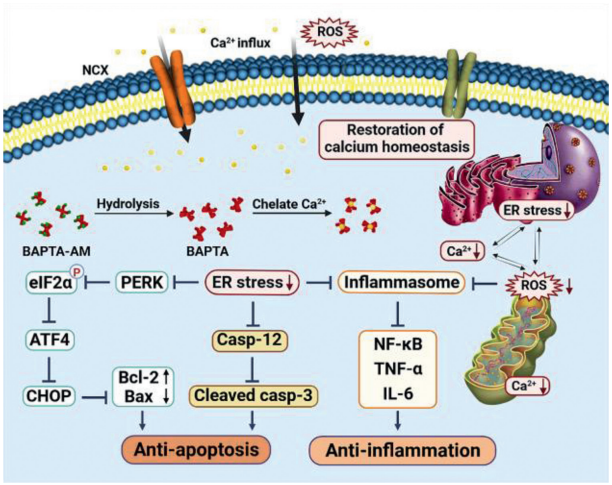

Fig. 5. Schematic illustration of the cellular regulatory mechanism of BA/mPLGA@Lipo-KTP NPs.

In conclusion, we fully verified the potential molecular mechanism of the acid-responsive lipid–mPLGA hybrid drug delivery system in alleviating AKI (Fig. 5), that is, blocking the activation of the ERS pathway and the inflammatory pathway, providing a reasonable explanation for the excellent anti-apoptotic and anti-inflammatory effects of the above NPs *in vivo*.

Even though the nano preparation was primarily distributed in the damaged kidney, there were still small accumulations in other major organs, so it was necessary to evaluate the organ toxicity of NPs in the systemic circulation. By measuring alkaline phosphatase (AKP), aspartate aminotransferase (AST), and alanine aminotransferase (ALT) (Figs. S9A–C in Supporting information), it can be found that these biomedical indicators were within the normal range, indicating the avoidance of systemic toxicity. Moreover, compared to the control group, no significant pathological changes were observed in tissue sections of major organs (liver, lung, and spleen) after BA/mPLGA@Lipo-KTP treatment (Fig. S9D in Supporting information), indicating that our nanoformulation was biosafe.

As a calcium chelating agent, BA-AM may trigger hypotension or cardiac arrest. When different doses of BA/mPLGA@Lipo-KTP were injected into healthy SD rats (BA-AM dose: 100, 200, 300 μg/kg *bw*), it was found that the preparation did not affect blood pressure and heart rate (Figs. S9E and F in Supporting information), even when the injection dose was as high as 300 μg/kg

bw, indicating that at the injection dose of 200 μg/kg *bw*, NPs did not cause cardiovascular problems [48–50]. These results indicated the preparation's exceptional biological safety and laid a foundation for future clinical translation.

To summarize, we developed a lipid-mPLGA hybrid drug delivery system that targets the pathogenesis of AKI and addresses the following key questions: (i) Efficient EE of hydrophobic drug BA-AM (up to 96.1%) and excellent storage stability (∼8 days); (ii) Dual target characteristics: passive target (size: <100 nm) and active target (KTP-targeted peptide modification); (iii) Slightly acid-responsive drug release: the CHEMS component in the phospholipid bilayer structure is an acidic cholesterol ester, whose configuration changes at low pH (pH: ∼6.5) to release the drug; (iv) Source blocking therapy: BA-AM was decomposed by intracellular esterase to unleash BA, quickly removing intracellular excess Ca^{2+}, restoring calcium homeostasis, thus promoting the oxidative stress balance, playing anti-inflammatory and anti-apoptosis roles, and finally promoting kidney function recovery.

Mechanically, this nano preparation can rapidly chelate Ca^{2+}, block ROS generation, rescue ERS, and inhibit the expression of key downstream apoptotic proteins (ATF4–CHOP–Bax, Casp-12–Casp-3). Furthermore, the nano preparation suppressed the expression of inflammatory factors (TNF-α, NF-κB, and IL-6), thus blocking the activation of downstream apoptotic factors.

In our experiments, the KTP-modified yolk-shell structure of mPLGA-liposome hybrid NPs not only remedied the defects of low encapsulation efficiency and instability when liposomes encapsulate extremely hydrophobic drugs BA-AM, but also well compensated for the shortcomings of PLGA NPs that were not easy to be modified and had short blood circulation time. Therefore, at such a low dose (BA-AM: 200 μg/kg *bw*), BA/mPLGA@Lipo-KTP accumulated at the injured kidney site through active and passive targeting in the long blood circulation, then released BA-AM/mPLGA nanoparticles in a slightly acidic inflammatory environment, which was then depolymerized by intracellular esterase. The BAPTA-AM was diffused and hydrolyzed to produce BAPTA, which chelated the overloaded intracellular Ca^{2+}, thus breaking the vicious cycle formed by Ca^{2+} and ROS, strongly inhibiting the apoptosis of renal cells, and rapidly restoring renal function to nearly normal levels. In addition, no acute cardiovascular adverse effects or organ toxicity were seen *in vivo*. We believe that our formulation holds great potential for the future clinical treatment of AKI.

Declaration of competing interest

The authors declare that they have no known competing financial interests or personal relationships that could have appeared to influence the work reported in this paper.

Acknowledgments

This work was supported by the Taishan Scholar Foundation of Shandong Province (No. tsqn202211065), Hainan Provincial Joint Project of Sanya Yazhou Bay Science and Technology City (No. 2021JJLH0037), the Natural Science Foundation of China (No. 82003673), the Fundamental Research Funds for the Central Universities (No. 202113049).

Supplementary materials

Supplementary material associated with this article can be found, in the online version, at doi:10.1016/j.cclet.2023.108434.

References

[1] F.C. Luft, Acta Physiol. 231 (2020) e13479.
[2] J.A. Kellum, J.R. Prowle, Nat. Rev. Nephrol. 14 (2018) 217–230.
[3] C. Ronco, R. Bellomo, J.A. Kellum, Lancet 394 (2019) 1949–1964.
[4] S. Peerapornratana, C.L. Manrique-Caballero, H. Gómez, J.A. Kellum, Kidney Int. 96 (2019) 1083–1099.
[5] S. Tandukar, P.M. Palevsky, Chest 155 (2019) 626–638.
[6] G. Fortrie, H.R.H. de Geus, M.G.H. Betjes, Crit. Care 23 (2019) 24.
[7] R. Chen, P. Ouyang, L. Su, et al., Chin. Chem. Lett. 33 (2022) 4610–4616.
[8] H. Tian, M. Wu, P. Zhou, et al., Ren. Fail. 40 (2018) 527–533.
[9] G. Zhang, H. Han, Z. Zhuge, et al., Redox Biol. 39 (2021) 101836.
[10] B.I. Ucar, G. Ucar, S. Saha, et al., Antioxidants 10 (2021) 823.
[11] S.J. Park, C. Li, Y.M. Chen, Am. J. Pathol. 191 (2021) 256–265.
[12] J. Ansari, G. Kaur, F. Gavins, Int. J. Mol. Sci. 19 (2018) 1211.
[13] H. Khanahmad, S.M. Mirbod, F. karimi, et al., Mol. Biol. Rep. 49 (2022) 11071–11079.
[14] K. Beider, E. Rosenberg, V. Dimenshtein-Voevoda, et al., J. Hematol. Oncol. 13 (2020) 158.
[15] Z. Fu, Q. Fan, Y. Zhou, et al., ACS Appl. Mater. Interfaces 11 (2019) 39574–39585.
[16] S. Li, D. Lu, J. Tang, et al., BioMed Res. Int. 2019 (2019) 7387803.
[17] J. Westman, G.F.W. Walpole, L. Kasper, et al., Cell Host Microb. 28 (2020) 798-812.e796.
[18] X. Zhang, Y. Wang, M. Chen, M. Zeng, Ecotoxicol. Environ. Saf. 208 (2021) 111391.
[19] T. Sun, G. Zhang, Z. Guo, et al., J. Control. Release 321 (2020) 483–496.
[20] L. Gong, X. Zhang, K. Ge, et al., Biomaterials 267 (2021) 120483.
[21] E.A. Ismail, N. Devnarain, T. Govender, C.A. Omolo, J. Control. Release 352 (2022) 1048–1070.
[22] T. Yoshitomi, Y. Nagasaki, Adv. Healthc. Mater. 3 (2014) 1149–1161.
[23] H. Yu, D. Liu, G. Shu, et al., Asian J. Pharma. Sci. 16 (2021) 432–443.
[24] V. Dave, K. Tak, A. Sohgaura, et al., J. Microbiol. Methods 160 (2019) 130–142.
[25] P. Dana, S. Bunthot, K. Suktham, et al., Colloids Surf. B: Biointerfaces 196 (2020) 111270.
[26] X. You, L. Wang, J. Zhang, et al., Chin. Chem. Lett. 34 (2023) 107720.
[27] G.W. Liu, J.W. Pippin, D.G. Eng, et al., Physiol. Rep. 8 (2020) e14545.
[28] J. He, H. Chen, W. Zhou, et al., Int. J. Pharma. 584 (2020) 119455.
[29] G. Wang, Q. Li, D. Chen, et al., Theranostics 9 (2019) 6191–6208.
[30] M. Abri Aghdam, R. Bagheri, J. Mosafer, et al., J. Control. Release 315 (2019) 1–22.
[31] K.L. Alatise, S. Gardner, A. Alexander-Bryant, Cancer Res. 81 (2021) 281.
[32] X. Duan, Y. Li, Small 9 (2013) 1521–1532.
[33] G. Liu, Y. Zhou, Z. Xu, et al., Chin. Chem. Lett. 34 (2023) 107705.
[34] P. Xin, S. Han, J. Huang, et al., Chin. Chem. Lett. 34 (2023) 108125.
[35] C.L. Edelstein, Biomarkers in Acute Kidney Injury, Biomarkers Kidney Dis., New York, 2017, pp. 241–315.
[36] H. Yu, T. Lin, W. Chen, et al., Biomaterials 219 (2019) 119368.
[37] G. Zhao, N. Li, M. Yin, M. Xu, J. Biomed. Nanotechnol. 17 (2021) 1754–1764.
[38] H. Boyacıoğlu, B.B. Yola, C. Karaman, et al., Appl. Surf. Sci. 578 (2022) 152093.
[39] J. Li, Q. Duan, X. Wei, et al., Small 18 (2022) 2204388.
[40] M. Yan, S. Shu, C. Guo, et al., Ann. Med. 50 (2018) 381–390.
[41] E. Martínez-Klimova, O.E. Aparicio-Trejo, T. Gómez-Sierra, et al., BioFactors 46 (2020) 716–733.
[42] X.M. Wei, S. Jiang, S.S. Li, et al., ACS Omega 6 (2021) 8958–8966.
[43] J.S. Mo, D. Choi, Y.R. Han, et al., Biomed. Pharmacother. 112 (2019) 108659.
[44] T. Habshi, V. Shelke, A. Kale, et al., J. Cell. Phys. 238 (2022) 82–93.
[45] Y. Song, L. Liu, B. Liu, et al., Pharmacol. Res. 165 (2021) 105371.
[46] P. Rojas-Franco, M. Franco-Colín, A.P. Torres-Manzo, et al., Ren. Fail. 41 (2019) 1001–1010.
[47] J. Bai, J. Zhao, D. Cui, et al., Sci. Rep. 8 (2018) 9173.
[48] Y. Wang, M. Pu, J. Yan, et al., ACS Nano 17 (2022) 472–491.
[49] Y.H. Lee, J.Y. Son, K.S. Kim, et al., Int. J. Mol. Sci. 20 (2019) 3709.
[50] J. Yan, Y. Wang, J. Zhang, et al., Small (2023), doi:10.1002/smll.202206936.